Tectonophysics, 69 (1980) 163—188
Elsevier Scientific Publishing Company, Amsterdam — Printed in The Netherlands

TERRESTRIAL HEAT FLOW IN THE TERTIARY BASIN OF CENTRAL SUMATRA

HUMBERTO DA SILVA CARVALHO [1], PURWOKO [2], SISWOYO [2], M. THAMRIN [2] and VICTOR VACQUIER [3]

[1] *Programa de Pesquisa e Pós-Graduaçá em Geofisica da UFBa, Instituto de Física, Rua Caetano Moura 123, Federaçáo, Salvador, Bahia (Brazil)*
[2] *Pertamina, Perwira 6, Jakarta (Indonesia)*
[3] *University of California, San Diego, Marine Physical Laboratory of the Scripps Institution of Oceanography, La Jolla, Calif. 92093 (U.S.A.)*

(Received February 9, 1979; revised version accepted January 17, 1980)

ABSTRACT

Carvalho, H. da S., Purwoko, Siswoyo, Thamrin, M. and Vacquier, V., 1980. Terrestrial heat flow in the Tertiary basin of Central Sumatra. Tectonophysics, 69: 163—188.

Heat flow at 170 locations in the Central Tertiary basin of Sumatra was determined from thermal gradients obtained from the extrapolated oil well bottom hole formation temperature and the assumed temperature of 80°F at the surface. The effective thermal conductivity of the whole rock column, by which the gradient is multiplied to get the heat flow was calculated from measurements on 273 specimens of the geologic section and inspection of 92 well logs. For the whole basin the gradient averaged 3.71 ± 1.04°F/100 ft (67.6°C/km) the conductivity 4.83 ± 0.31 mcal $^{\circ}C^{-1}$ cm^{-1} sec^{-1}, giving an average heat flow of 3.27 ± 0.93 10^{-6} cal cm^{-2} sec^{-1} which is about twice the world average. The gradient and the heat flow vary inversely with the depth of the wells most of which bottom in the pre-Tertiary basement. This may result from the basement rocks being several times more conductive than the sediments. Mocel calculations on a narrow heat-flow anomaly which rises from a base level of 3.2 HFU to 8.8 HFU suggest that it can be caused by the intrusion less than 55,000 years ago of an igneous plug or laccolith no deeper than 3 km and 2.2 to 4.6 km wide.

Using the gradients from the SEAPEX Geothermal Gradient Map and assuming a conductivity of 5 mcal cm^{-1} $^{\circ}C^{-1}$ sec^{-1}, the heat flow in the North Sumatra basin, the South Sumatra Basin, Sunda Strait and West Java is 2.5 HFU, while in Java east of 110°E longitude it drops to 1.9 HFU. Since subduction off Sumatra dates back at least to the Cretaceous, compression of the Asian plate against the Benioff zone is preventing the opening of a back-arc basin. This does not preclude the possibility of occasional periods of crustal tension corresponding perhaps to episodes of transgression which allow magma to rise into the rocks underlying the basin.

INTRODUCTION

In the theory of plate tectonics, the concentration of volcanoes along the border of the Pacific Ocean, the so-called "ring of fire" is accounted for by

0040-1951/80/0000-0000/$02.25

magmatism associated with the subducting slab of oceanic lithosphere. The magma for the volcanism is generated from the material of the asthenosphere by the fluxing action of the water given off by the subducting slab. Originally the water entered the slab where it was formed at a submarine spreading ridge. From towing thermometers and from observation and sample collection with deep-diving submersibles we have direct evidence (Weiss et al., 1977) that at spreading ridges sea water penetrates the extruding basalt, cooling it and causing extensive hydration of olivine and other minerals. The width and character of the low heat-flow anomaly at the very crest of spreading ridges indicates penetration of sea water several kilometers into the extruding basalt (Lister, 1972; Williams et al., 1974). When the subducting slab, as it descends into the hot asthenosphere, heats up above 500° C at the depth of about 80 km, it gives off water from the dehydration of serpentine and other hydrated minerals (Anderson et al., 1976). Ringwood (1977) writes: "Water . . . will be introduced into the wedge overlying the Benioff zone continually throughout the 80—300 km depth interval". In the case of the Sunda (Indonesia) island arc, the dip of the Benioff zone is only 30° (Fitch, 1970), which would bring magmatic diapirs mobilized by water given off by the descending slab, to rise as far as 400 km away from the trench, i.e., under the sedimentary basins of Sumatra. We may expect, therefore, to find high heat flow in the back-arc region of the Sunda island arc even though there is no deep marginal sea behind it, where heat flow is high in most cases such as the Seas of Japan, or Okhotsk.

According to Uyeda and Kanamori (1979), subduction zones may be classified according to whether or not large shallow intraplate earthquakes are associated with them. Compared to the speed of plate motions, they regard the subducting slab as relatively fixed in the asthenosphere in the direction perpendicular to its strike. The great shallow earthquakes occur when the landward plate has a component of motion toward the subducting slab, like the west coast of South America. When it moves away from the slab, large shallow earthquakes are missing and a marginal sea is formed like back of the Mariana trench. Subduction at the Sunda island arc dates as far back as the Cretaceous (Katili, 1975). During all that time no deep marginal sea has formed (Hamilton, 1979), suggesting that the crust landward of the descending slab has been in compression most of the time. The pronounced pre-trench topographic swell with its slight rise of heat flow also indicates compression (Vacquier and Taylor, 1966).

With the preceding discussion in mind, we shall examine the distribution of anomalous heat flow in the Central Sumatra basin for clues leading to an explanation of its origin.

GEOLOGY

The sedimentary basins of Sumatra and western Java are shown in Fig. 1. The plate boundary is given by the axis of the deep sea trench and the rota-

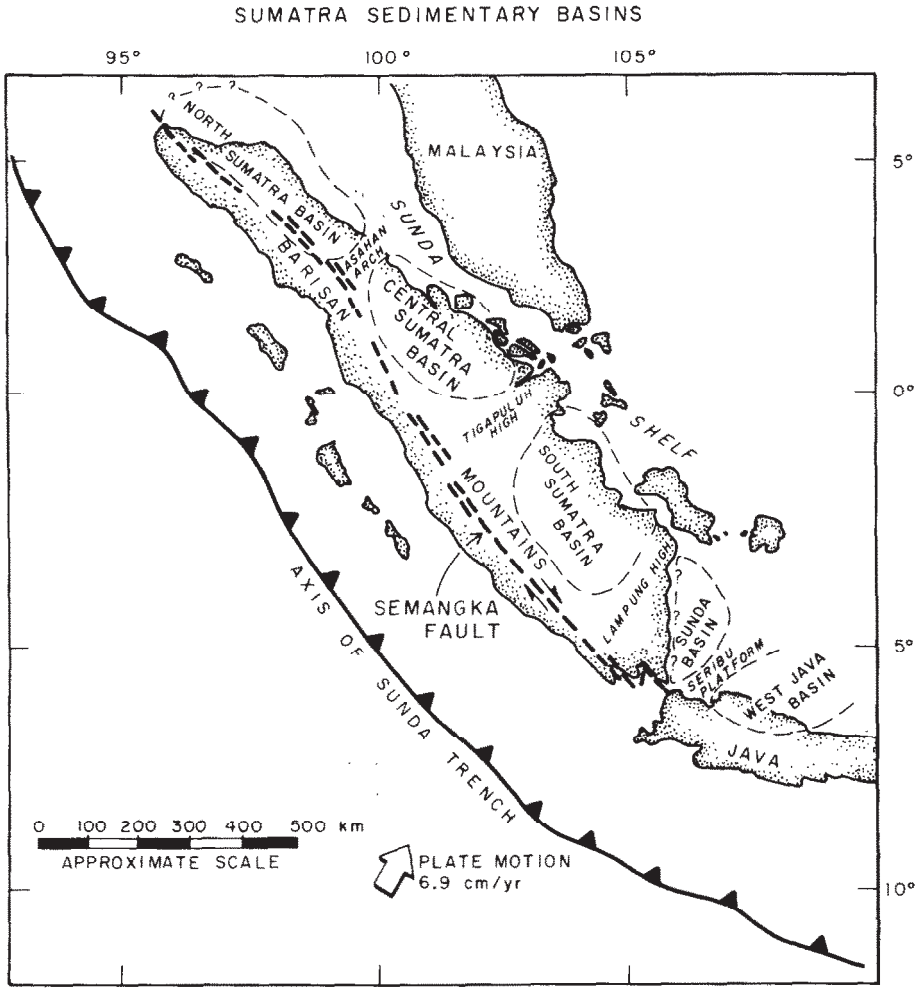

Fig. 1. Location of petroliferous basins of Sumatra and West Java. The relative plate motion of 6.9 cm/yr is shown by the fat arrow.

tion of the Indian plate relative to the Eurasian plate about the pole at 29°N 27°E (Morgan, 1971) is shown by the fat arrow. The rate of rotation is 6.5 10^{-7}°/yr corresponding to a consumption rate of 6.9 cm/yr at western Java.

The geology of the Central Sumatra basin is described by Mertosono and Nayoan (1974), by Mertosono (1975) and Hamilton (1979). The block faulting of this Tertiary basin is controlled by a pre-Tertiary northerly grain and by a younger northwesterly trend parallel to the present boundary between the Indian and Asian plates. The Semangka fault with its right lateral displacement strikes parallel to this convergent plate boundary and extends the whole length of the southwestern portion of Sumatra. The Barisan moun-

TABLE I

Age of stratigraphic units in the Central Sumatra basin

Name of stratigraphic unit	Age
Minas/Alluvium	Quaternary
Petani	Pliocene—Mid-Miocene
Telisa	Mid-Miocene—Early Miocene
Sihapas group	Early Miocene
Duri	Early Miocene
Bekasap	Early Miocene
Bangko	Early Miocene
Menggala	Early Miocene
Pematang	Paleogene
Basement	Pre-Tertiary

tains associated with this fault form the southwestern border of the basin. Most of the rocks filling the basin crop out along the mountain front where they can be sampled.

Cretaceous orogeny left the basement of the Central Sumatra basin with numerous troughs and grabens striking NNW, which later during the early Tertiary were filled with clastic and marine deposits during several epochs of transgression and regression. The normal faults bounding these structures have throws up to 7000 ft. The rocks constituting the pre-Tertiary basement are greywacke, quartzite, and occasionally granite. During the Miocene the present structural trend began to cause folding and faulting, with a NW strike that one would expect from compression due to subduction of the Indian Ocean floor. These movements became more intense during the Plio-Pleistocene orogeny when magma was injected at scattered locations mostly close to the Barisan mountains, giving rise to volcanoes, laccoliths and solfataras on their eastern flank and also lifting the intramontane basins of the Barisan range to high elevations. During the Quaternary, fluvial deposits were laid unconformably on the Tertiary sediments.

In presenting our measurements on thermal conductivity, the names of the stratigraphic units will be mentioned. From the discussion of the structure of the basin it is evident that these units vary in thickness over such a wide range that it would be meaningless to assign to them some average thickness, while to tabulate their thickness in each well would be unnecessarily cumbersome. Table I lists the formation names in order of increasing age.

MEASUREMENTS OF THERMAL CONDUCTIVITY

Heat flow is the product of the temperature gradient by the thermal conductivity. In this work we used the customary method of determining the

temperature gradient as described in the Schlumberger well logging manual or its equivalent given by Dowdle and Cobb (1974). It consists of calculating by extrapolation the undisturbed formation temperature from at least two measurements of temperature taken at different times at the same depth near the bottom of the hole which are routinely taken during the well-logging procedure. The mean temperature at the surface, obtained from meteorological records, is then subtracted from the formation temperature and the difference divided by the total depth. Since this procedure determines the gradient over the entire depth of the well, one needs to calculate the mean thermal conductivity likewise from the bottom clear to the surface. We were able to do this because fortunately some samples of the upper part of the section were available from a few exploratory holes.

The thermal conductivity of 273 representative specimens from the stratigraphic units listed in Table I was measured by the hot wire method described in the Appendix. They were grouped by rock type from their visual appearance into shale, sandstone, siltstone and basement, the latter

TABLE II

Average thermal conductivity by rock type

Rock	Serial number	No. of samples	⟨K⟩ (10^{-3} cal cm^{-1} $°C^{-1}$ sec^{-1})	Standard deviation ±
Shale	1—129	63	4.23	0.88
	130—172	32	4.31	0.55
	173—300	52	4.38	0.73
	301—333	6	3.86	0.96
Weighted mean		153	⟨4.28⟩	0.76
Sandstone	1—129	34	7.52	1.33
	130—172	(11)	(5.65)	1.31
	173—300	31	7.48	1.49
	300—333	21	7.36	1.30
Weighted mean		86	⟨7.47⟩	1.38
Claystone only from Pematang		10	⟨7.84⟩	1.75
Graywacke		18	⟨9.68⟩	2.34
Quartzite		6	⟨15.42⟩	0.37
"Basement"			12.55	
		273		

Serial numbers 130—172 are from Telisa outcrop. ( ) were not used for averaging.

consisting of greywacke or quartzite. When in the well records the word "Basement" occurred, we used the average of the two. With the exception of eleven samples of sandstone from the Telisa formation cropping out in a stream bed, the averages of the four sets of specimens gave concordant values of thermal conductivity (Table II).

From the average values of conductivity for rock types listed in Table II, we calculated the average conductivity of the stratigraphic units of Table III by inspecting electric well logs from 92 wells. Taking a particular stratigraphic unit, the boundaries of which are marked on the well log record, the total thicknesses of shale and sandstone in the stratigraphic unit were determined from the amplitude of the spontaneous potential (SP) trace. Attempts should be made in the future to refine this admittedly crude division so as to allow for intermediate types, e.g., sandy shales and shaly sands. Perhaps this can be done by assigning intermediate values of spontaneous potential to these types of rock. The method could be refined further by taking into account porosity and whether gas, oil or water is the saturating fluid (Carvalho and Vacquier, 1977), factors that also affect the amplitude of the SP trace. Because in sedimentary basins the average conductivity is largely determined by the greater thickness of the poorly conducting rocks (usually shales), differences in the conductivity of the more conducting sandstones caused by shaliness, porosity and saturating fluid are relatively minor. As a rule, the contribution of the basement rocks to the average conductivity was less than 2%.

To calculate the mean conductivity of a particular stratigraphic unit, let the individual rock types with conductivities K_1, K_2, K_3 ... have total thicknesses d_1, d_2, d_3 ... as determined from the electric log or well file. The mean conductivity of the stratigraphic unit:

$$\langle K \rangle = \left[\left(\frac{d_1}{K_1} + \frac{d_2}{K_2} + \frac{d_3}{K_3} + \ldots \right) \frac{1}{d_1 + d_2 + d_3 + \ldots} \right]^{-1} \tag{1}$$

The stratigraphic units of Table I appear with their mean conductivity values in Table III. They were determined at 23 different locations plotted on the map of Fig. 2 for a total of 92 wells. With the exception of one value, the spread of the conductivities for a particular stratigraphic unit is small. The mean conductivity of stratigraphic units increases with formation age, reflecting the greater thickness of sandstones in the older strata. They range from $4.26 \cdot 10^{-3}$ to $6.69 \cdot 10^{-3}$ cal $cm^{-1}\,°C^{-1}\,sec^{-1}$.

The mean thermal conductivity for the whole rock column penetrated by the well is calculated by the same method, the conductivities being the average conductivities of the stratigraphic units given by Table III, and d_1, d_2 ... their individual thicknesses.

The thicknesses of the stratigraphic units in wells the electric logs of which were not examined, were gotten from the well files and the mean conductivities of the stratigraphic units in Table III. All conductivity values are entered in the fourth column of Table IV where the data from which the

TABLE III

Thermal conductivity of stratigraphic units (mcal cm^{-1} $°C^{-1}$ sec^{-1})

Location on map of Fig. 3	No. of wells	Minas	Petani	Telisa	Duri	Bekasap	Bangko	Menggala	Pematang
32a	4			4.39		5.54			
65	1			4.38		5.87			
67	3	4.29	4.29	4.38		5.22			
68	10		4.76	4.92		5.76			
74	10	(5.85)	4.72	4.52		5.43			
75	1	4.29	4.31	4.44		5.23	6.78		
116	11		4.44	4.98		6.04			5.59
139	2		4.35	4.40		5.77	5.36		
153	1	4.29	4.34	4.34		6.16			
155	3	4.29	4.44	4.34		6.32	5.71		6.20
112a	2	4.29	4.35	4.58		5.75	5.32		4.84
112	4	4.21	4.25	4.39		5.53		6.65	5.97
111	2	4.21	4.25	4.51		5.53	5.54	6.95	5.29
85	7	4.33	4.34	4.51	4.52	5.83	5.38	6.41	4.50
83	1	4.29	4.32	4.81	4.49	6.09	5.40	6.65	5.26
84	5	4.21	4.28	4.89	4.60	6.74	5.65	6.90	5.19
86	2	4.21	4.23	4.41	4.75	6.12	5.58	6.56	5.52
48	1		4.32	4.39	4.91	6.21	4.78	7.03	4.65
46	7		4.30	4.87	5.13	6.08	4.92	7.11	7.44
44	1		4.35	4.48	5.44	5.99	5.22		
41	8		4.38	4.98	5.50	6.25	5.78		7.48
26	4	4.21	4.28	4.63	5.40	5.89	5.99	6.11	4.21
148	2		4.64	4.37		6.12			5.68
	92								
Weighted mean		4.26	4.44	4.51	4.97	5.89	5.48	6.69	5.42

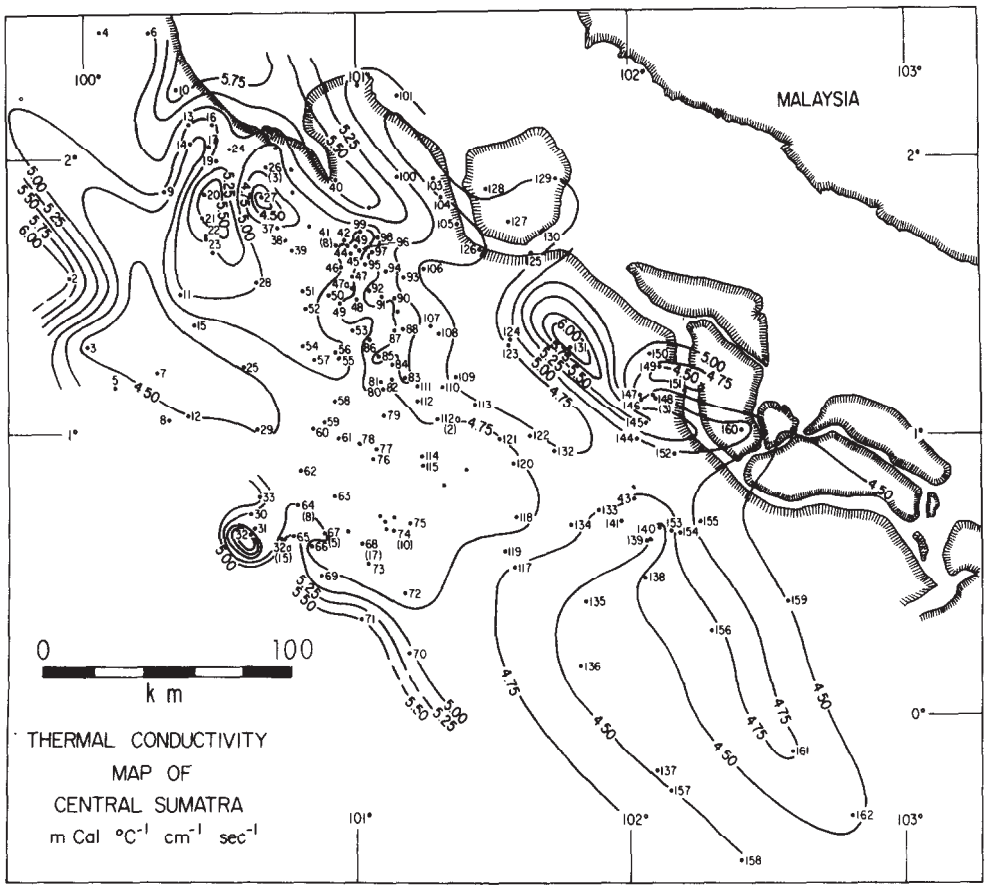

Fig. 2. Thermal conductivity map of Central Sumatra Basin. The numbers refer to locations for which Table IV lists depth, gradient, conductivity and heat flow. Contour interval is 0.25 mcal $°C^{-1}$ cm^{-1} sec^{-1}.

conductivity map (Fig. 2) and the heat flow map (Fig. 3) have been drawn are listed. Column 1 of the table gives the serial number of the location plotted on the map of Figs. 2 and 3. The conductivity values were contoured on Fig. 2 with a contour interval of $0.25 \cdot 10^{-3}$ cgs which is smaller than the uncertainty of the data, so that accuracy of representation is not lost by not entering the individual conductivities on the map. A few data points are not listed in Table IV, and those are mostly the ones for which the temperature gradient was missing. In Table IV the thermal conductivity of 170 wells of Fig. 2 is listed averaging 4.83 ± 0.31 mcal cm^{-1} sec^{-1} $°C^{-1}$. As previously noted, the differences between the individual values and the average in addition to errors of measurement, are caused by relative amounts of shale and sand, which depends on regional location and local structure.

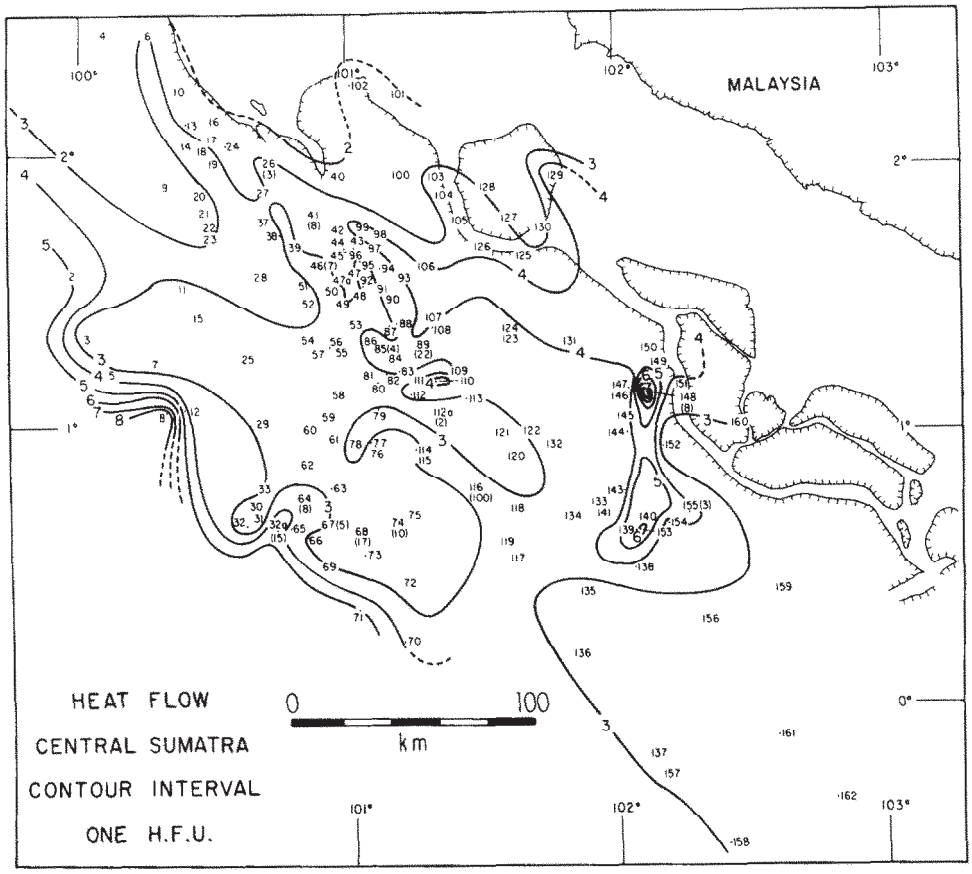

Fig. 3. Heat flow in Central Sumatra basin contoured with an interval of one HFU (10^{-6} cal cm^{-2} sec^{-1}). The numbers are locations for which Table IV gives the complete data.

TEMPERATURE GRADIENTS

The temperature gradients were obtained from the temperature measurements recorded on the well logging recordings and an assumed temperature of 80° F at the surface. Some calculations were done according to the procedure of the Schlumberger well logging manual, others by the equivalent method of Dowdle and Cobb (1974). Because of cooling by the circulating fluid, the temperature T at the bottom of the well rises after circulation is stopped prior to logging. Let T_i be the undisturbed formation temperature we seek, t_k the circulation time, Δt the time after circulation ceases, and C a constant, then:

$$T = T_i - C \ln\left(\frac{t_k + \Delta t}{\Delta t}\right)$$

TABLE IV

Temperature gradient, thermal conductivity and heat flow for locations numbered on maps of Figs. 2 and 3

Serial no. of locations on Figs. 2 and 3 *	Total depth (ft)	Temp. grad. (°F/100 ft) **	Thermal conductivity (mcal cm^{-1} $°C^{-1}$ sec^{-1})	Heat flow (HFU)
1	1876	2.9	5.03	2.66
2	1812	4.89	6.07	5.41
3	4157	3.4	4.50	2.79
4	7135	2.2	5.08	2.04
5	2430	5.0	4.57	4.16
6	5140	3.24	5.13	3.03
7	4500	3.1	4.48	2.53
8	899	10.5	4.55	8.71
9	3161	2.52	5.00	2.35
10	5546	2.6	5.92	2.81
11	4092	3.24	4.99	2.95
12	1946	5.0	4.51	4.11
13	4140	3.0	5.00	2.73
14	4039	3.84	4.80	3.36
15	4344	3.42	4.53	2.82
16	5177	3.0	4.91	2.68
17	3192	3.3	4.98	3.00
18	1899	4.28	4.71	3.67
19	2440	3.58	5.06	3.30
20	1386	2.75	5.64	2.83
21	4426	2.75	5.42	2.72
22	3495	2.6	5.28	2.51
23	3088	3.67	5.23	3.50
24	6078	2.65	5.12	2.47
25	5296	3.24	4.51	2.66
26	4103	3.69	4.83	3.23
27	3952	3.42	4.12	2.57
28	2356	4.07	5.09	3.78
29	5676	2.92	4.49	2.39
30	1600	3.46	4.70	2.96
31	1475	3.12	4.73	2.69
32	1626	3.35	3.99	2.44
32a(15)	1180	5.42	4.77	4.71
33	3247	5.15	5.03	4.72
34	4406	3.2	4.87	2.84
35	6128	1.9	5.33	1.85
36	5707	3.1	5.01	2.83
36	4923	3.42	4.94	3.08
37	3000	3.7	4.93	3.32
38	2620	3.69	4.97	3.34
39	7517	3.28	4.96	2.97
40	1527	2.65	5.56	2.69
41(8)	3932	3.95	5.08	3.17
41	2935	3.8	4.75	3.29

TABLE IV (continued)

Serial no. of locations on Figs. 2 and 3 *	Total depth (ft)	Temp. grad. (°F/100 ft) **	Thermal conductivity (mcal cm^{-1} $°C^{-1}$ sec^{-1})	Heat flow (HFU)
42	3241	3.85	4.76	3.34
43	2460	4.3	4.53	3.55
44	3070	4.35	4.74	3.76
45	3101	4.58	4.64	3.87
46(7)	3600	3.85	4.85	3.40
47	3496	4.19	4.77	3.64
47	3699	3.5	4.73	3.02
48	4498	3.6	4.88	3.20
49	5450	2.70	4.79	2.36
49		2.8		
50	4703	2.76	4.72	2.37
51	4115	3.7	4.85	3.27
52	4043	3.63	4.80	3.18
53	5664	3.3	4.74	2.85
54	7477	3.2	4.81	2.81
55	8163	3.07	4.78	2.67
56	8520	3.24	4.79	2.83
57	7112	3.38	4.76	2.93
58	6543	3.47	4.64	2.93
59	6626	3.23	4.62	2.72
60	6658	2.9	4.60	2.43
61	6277	3.0	4.64	2.54
62	6696	2.75	4.64	2.33
63	7071	3.24	4.62	2.73
64(8)	1155	4.38	4.79	3.82
65	1309	3.6	5.12	3.36
66	2176	3.4	4.63	2.87
67(5)	1970	4.01	4.53	3.32
68(17)	5607	2.87	4.96	2.59
69	1638	4.2	4.77	3.65
70	3164	3.6	5.17	3.39
71	1841	4.94	5.57	5.02
72	4691	3.2	4.58	2.67
73	4376	2.92	4.58	2.44
74(10)	5040	3.31	4.96	2.99
75	6142	3.35	4.51	2.75
76	6073	3.55	4.53	2.93
77	5992	2.55	4.56	2.12
78	6356	3.75	4.62	3.16
79	6910	3.7	4.54	3.06
80	6670	3.2	4.69	2.74
81	7096	3.3	4.79	2.88
82	7701	3.0	4.84	2.65
83	6545	3.3	5.22	3.14
84	6291	3.17	4.99	2.88
84	5142	3.0	4.90	2.68

TABLE IV (continued)

Serial no. of locations on Figs. 2 and 3 *	Total depth (ft)	Temp. grad. (°F/100 ft) **	Thermal conductivity (mcal cm^{-1} $°C^{-1}$ sec^{-1})	Heat flow (HFU)
84	3394	3.26	4.97	2.95
85(4)	6500	3.72	4.70	3.18
86	4680	2.63	4.89	2.44
87	3597	2.79	4.81	2.45
88	2610	3.6	5.18	3.40
89(22)	735	4.30	(4.80)	(3.75)
89	1999	3.6	5.05	3.31
90	2397	3.7	4.96	3.34
91	4375	2.95	5.05	2.72
92	5221	3.23	5.10	3.00
93	1454	3.77	4.91	3.37
94	2264	3.52	5.07	3.25
95	4002	3.3	4.82	2.90
96	2950	4.58	4.61	3.85
97	4216	3.3	5.20	3.13
98	2101	4.8	4.81	4.21
99	2555	4.8	4.72	4.13
100	2111	2.45	5.17	2.31
101	2487	2.4	4.89	2.14
102	1922	2.87	4.93	2.58
103	1329	4.57	4.62	3.85
104	1624	3.6	4.87	3.20
105	1993	3.96	4.80	3.46
106	3328	3.96	4.68	3.38
107	2000	5.09	4.76	4.42
108	2378	4.44	4.80	3.88
109	2942	3.24	4.60	2.72
110	1980	5.0	4.91	4.47
111	5814	2.94	4.96	2.66
112	4281	3.46	4.82	3.04
112a	4020	3.47	4.81	3.04
112(3)	3722	3.0	4.66	2.55
113	1818	3.4	4.78	2.96
114	4560	3.42	4.62	2.88
115	3825	3.69	4.64	3.12
116(100)		3.77	4.94	3.77
117	3200	4.2	4.59	3.51
118	3249	3.9	4.54	3.23
119	3811	3.74	4.72	3.22
120	5027	3.05	4.65	2.59
121	4121	3.35	4.66	2.85
122	4963	3.26	4.98	2.96
123	2250	4.2	4.73	3.62
124	1804	4.26	4.99	3.87
125	1473	4.1	4.70	3.51
126	1479	4.48	4.86	3.97

TABLE IV (continued)

Serial no. of locations on Figs. 2 and 3 *	Total depth (ft)	Temp. grad. (°F/100 ft) **	Thermal conductivity (mcal cm^{-1} $°C^{-1}$ sec^{-1})	Heat flow (HFU)
127	942	4.2	4.64	3.55
128	1847	3.4	4.91	3.04
129	2932	3.57	4.64	4.32
130	3591	3.11	4.60	2.61
131	1288	4.1	6.20	4.63
132	3410	4.03	4.82	3.54
133	2623	4.35	4.49	3.56
134	4241	4.1	4.87	3.64
135	3927	3.6	4.46	2.91
136	4254	3.1	4.44	2.51
137	5490	3.0	4.48	2.45
138	2856	4.7	4.57	3.91
139	2248	7.1	4.56	5.90
140	1634	8.0	4.46	6.50
141	2893	4.17	4.58	3.48
142	2513	5.2	4.67	4.43
143	4820	3.65	4.87	3.24
144	2784	3.81	4.93	3.42
145	2594	4.7	5.50	4.71
146	2532	3.3	5.08	3.06
147	1340	4.36	4.61	3.66
148(8)	1111	8.47	5.71	8.82
149	2003	5.58	4.46	4.54
150	2834	5.8	4.79	4.52
151	3847	3.9	4.74	3.37
152	5628	3.2	4.78	2.79
153	2229	4.35	4.61	3.59
154	3003	4.4	4.77	3.83
155(3)	3337	4.04	4.69	3.44
156	5900	3.13	4.73	2.70
157	5026	3.4	4.61	2.86
158	6570	3.2	4.72	2.75
159	3565	3.4	4.50	2.79
160	5754	3.37	4.95	3.04
161	6094	2.55	4.77	2.22
162	2967	3.35	4.53	2.77
Total number		172	170	170
Average and standard deviation		3.71 ± 1.04	4.83 ± 0.31	3.27 ± 0.93
After deletion of items exceeding one standard deviation:				
Total number		144		147
Average and standard deviation		3.56 ± 0.53		3.06 ± 0.43

* ( ) denotes no. of wells averaged.
** 1°F/100 ft = 18.23 °C/km.
*** 1 HFU = 10^{-6} cal cm^{-2} sec^{-1}.

Plotting T on semi log paper against $(t_k + \Delta t)/\Delta t$ and extrapolating the straight line to unity yields T_i. The formula has been arrived at empirically and verified experimentally. Having obtained the formation temperature, we subtract the mean annual surface temperature. What we shall call the temperature gradient is this temperature difference divided by the total depth. Because the conductivity varies with the nature of the rock as previously discussed, the gradient along the hole is not constant, so that the actual underground temperatures at intermediate depths cannot be accurately calculated by just using the average gradient. In fact, stratigraphic correlation has been done by Beck (1976) and by Conaway and Beck (1977), from detailed temperature logging of cased bore holes.

The calculated temperature gradient depends on the assumptions that the average surface temperature has remained constant during the time that heat takes to diffuse from the bottom of the wells to the surface (20,000—200,000 yrs), and that there is no upward transfer of heat due to circulation of rain water. As we have mentioned previously, the subduction zone is well anchored in latitude and also the time involved is short — no more than 200,000 yrs. The bottom hole temperatures (BHT) are about 75° F (42° C) greater than the surface temperature. At the equator, an average climatic temperature change greater than 10% of this figure is unlikely.

The circulation of meteoric water in the upper part of the geologic section would increase the conductivity and therefore the heat flow above the calculated values. Some flow of water there must be happening so that the actual heat flow is greater than we have calculated. However, one would expect water circulation to be different from place to place, causing a greater scatter of values than is observed. Because the scatter of observed values is small, the effect of vertical motion of water must be negligible.

The temperature gradient does depend, however, on the depth of the wells or of the basement, as shown in Fig. 4, despite the fact that the mean conductivity is greater for the shallower wells.

To see whether perhaps the extrapolated formation temperatures are dependent on the depth through some unexpected connection and to evaluate the precision of the values of the gradients, the data from which Fig. 4 was drawn, are tabulated in greater detail in Table V. The locations of these fields, given in the first column of Table V, appear as numbered points on the maps of Figs. 2 and 3. As can be seen from the map of Fig. 3, the average depths of the seven fields in Fig. 4 and Table V are irregularly distributed, the depths depending mostly on local structure rather than on geographic position. The second column of Table V gives the number of wells from which the data were taken, 179 in all. The temperature gradient with its standard deviation calculated from the extrapolated formation temperature (Dowdle and Cobb, 1974) appears in the fourth column, while the gradient from the last measured temperature is in column five. Dividing the numbers in column five by the numbers in column four (column six), shows that this ratio is independent of the depth, so that if no account were taken of the

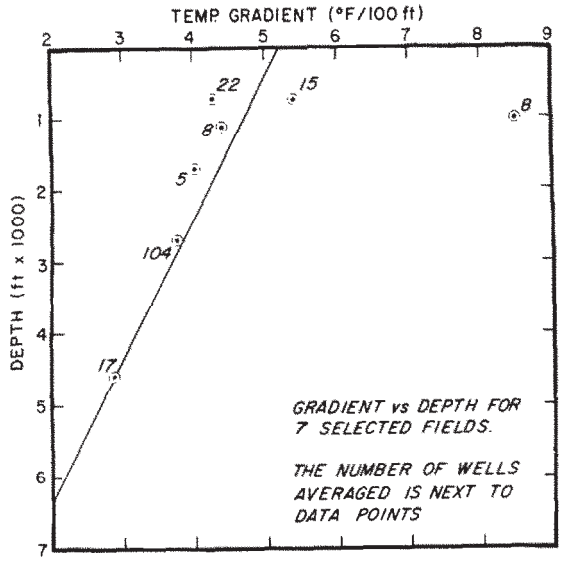

Fig. 4. Temperature gradient in °F/100 ft vs. depth in ft for seven fields. The number of wells from which data were averaged is given next to the plotted points.

cooling caused by circulating the well prior to logging, the gradients would be only 15% lower. This furnishes a criterion for rejecting data. When the ratio of the two gradients is less than 0.80, the value is regarded as suspect. If the departures from the mean follow the normal distribution, and they

TABLE V

Precision of temperature gradients for seven fields

Field location on Figs. 2 and 3	Number of wells	Average depth (ft)	Gradient from extrapolated formation temperature (°F/100 ft) *	Gradient from last measured temperature	Ratio of col. 5/ col. 4	Probable error of value from one well (°F/100 ft)*
89	22	735	4.30 ± 1.28	3.66 ± 0.90	0.85	0.58
32a	15	762	5.42 ± 1.30	4.62 ± 0.21	0.85	0.51
148	8	1024	8.47 ± 1.59	6.56 ± 1.34	0.77	1.07
64	8	1131	4.38 ± 0.93	3.77 ± 0.74	0.86	0.47
67	5	1724	4.01 ± 0.50	3.45 ± 0.36	0.86	0.44
116	104	2714	3.77 ± 0.65	3.14 ± 0.33	0.83	0.28
68	17	4589	2.87 ± 0.25	2.45 ± 0.17	0.85	0.12
	179					

* Multiply by 18.23 to obtain °C/km.

actually did in the case of the Minas Field where we examined the data from 100 wells, one can calculate the probable error of a single gradient determination which is given in the last column of Table V. It means that, without regard to sign, errors greater than this value and those that are smaller, have equal probability of occurring, so that if we had a great number of determinations there would be about as many errors with absolute values greater than the probable error, as there would be smaller. If in Table V we assume that the gradient from the extrapolated formation temperature is the correct value and discard the data from fields where fewer than 15 wells were used, the probable error is about 8.6%. So that we can say with fair assurance that a probable error smaller than 10% can be incurred from an acceptable gradient in the case of a heat flow value obtained from a single well. The third column of Table IV gives 172 gradients at locations numbered on the heat flow map of Fig. 3. They average 3.71 ± 1.04°F/100 ft (67.6 ± 19.0°C/km). After deletion of entries exceeding one standard deviation, 144 values that are left average 3.56 ± 0.53°F/100 ft (64.9 ± 9.7°C/km). As in the case of the conductivity, a portion of the departures from the average is real. For example, the gradient of 8.47 at location 148 is the average from eight wells with a standard deviation of 1.59.

HEAT FLOW

The last column of Table IV gives the heat flow in HFU for the numbered locations of the map of Fig. 3. The overall average of 170 values at 162 locations is 3.27 ± 0.93 HFU. Deleting the entries which depart from this figure by more than one standard deviation, like the unrepresentative value at location 148, leaves 147 values averaging 3.06 ± 0.43 HFU. This is higher than the average heat flow in all the back-arc basins around the Pacific Ocean (Watanabe et al., 1977).

The heat flow map of Fig. 3 has been contoured on the assumption that the heat flow follows the trend of the Barisan mountains, with heat flow rising steeply to the southwest. Although the 5 HFU contour depends on only three widely spread points, the 4 and the 3 HFU contours depend on more values and run parallel to it. The center of the basin is cooler: between 2 and 3 HFU. Proceeding farther to the northeast, the heat flow rises over the northeastern rim of the basin to over 4 HFU. From there it drops, as indicated by a few scattered values at the northeastern edge of the data. Most of the structures in the basin also strike NW.

MAGMATIC DIAPIRISM

On Fig. 3, a narrow feature strikes N—S between locations 138 and 149, reaching a value of 8.8 HFU at location 148. Unfortunately, the data points are too sparse to define the shape of the heat flow anomaly; all we know is that it rises from 3.2 to 8.8 HFU in about 5 km. This narrowness and high

amplitude indicate both recent origin and a shallow source of heat. To estimate these quantities we have calculated the thermal effects of an igneous intrusion which has stoped its way into the pre-Tertiary basement and then solidified at a certain depth. We do not regard circulation of hot water as a likely source of the high heat flow, even though it would be noteworthy indeed to have commercial deposits of petroleum maturated by a hot spring. Where we have direct evidence for the circulation of hot water, the heat flow values scatter from zero to over 30 HFU (Williams et al., 1974), whereas at location 148 we have eight wells with an average temperature gradient of $8.47 \pm 1.59°$ F/100 ft. Also the well-documented extension of this anomaly to the south suggests the presence of a more extended source than hot springs, such as an igneous intrusion which occurred during the late stage of the Barisan uplift.

We have used the calculation of Simmons (1967) of the heat flow over a rectangular parallelopiped for estimating the maximum age and the maximum depth of burial. As is often the case in geophysics, the model gives the limiting value of some parameters on one side only. Our model fails to give the shallowest depth of burial. The latter has to be fixed by other considerations such as there should be room enough for oil-bearing rocks. We do not claim that the actual intrusion is rectangular. All that the calculations are intended to demonstrate is that rectangular models having the same values of physical constants but widely different dimensions are younger than about 55,000 years and cannot lie deeper than about 3 km (see Table VI). From

TABLE VI

Dimensions and age of intrusion models
(See Figs. 5 and 6. $k = 0.01195$)

Model no.	$kt \cdot 10^{10}$	x_2 (km)	y_2 (km)	z_1 (km)	z_2 (km)	$t \cdot 10^3$ yrs
1	1.00	2.31	∞	0.5	0.90	26.5
2	1.00	2.31	∞	1.0	1.30	26.5
3	1.00	2.31	∞	2.5	3.13	26.5
4	1.00	2.31	∞	2.90	∞	26.5
5	1.00	2.31	2.31	0.5	0.94	26.5
6	1.00	2.31	2.31	1.0	1.33	26.5
7	1.00	2.31	2.31	2.5	3.24	26.5
8	1.00	2.31	2.31	2.82	∞	26.5
9	2.05	1.11	∞	0.5	2.08	54.4
10	2.05	1.11	∞	1.0	2.37	54.4
11	2.05	1.11	∞	2.5	4.48	54.4
12	2.05	1.11	∞	2.82	∞	54.4
13	2.05	1.11	1.11	0.5	4.87	54.4
14	2.05	1.11	1.11	0.86	∞	54.4

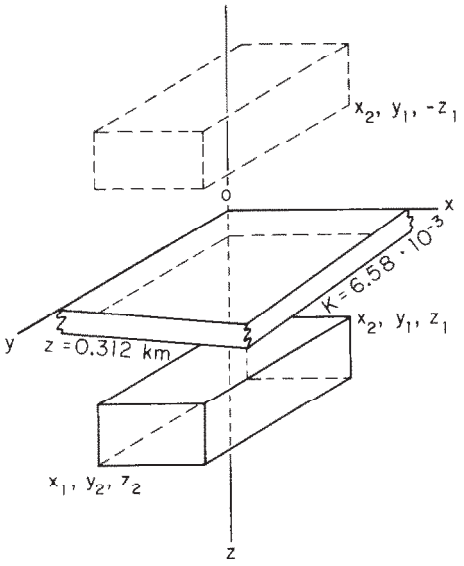

Fig. 5. Parameters for a rectangular intrusion that could account for the heat flow anomaly at 1°N 102°E on the map of Fig. 3. The model calculations are summarized in Table VI.

this we propose without proof that models of other geometric shape such as ellipsoids or cylinders would not give substantially different maximum ages and depths of burial.

The theory of the model assumes that intrusion is instantaneous when compared to the time it takes heat to diffuse to the depth of the wells. As is usual in such calculations, the thermal conductivity and diffusivity of the intrusion are assumed to be the same as for the country rock and constant in time. The geometry of the model is shown on Fig. 5. The origin of coordinates is over the center of the body so that $x_2 = -x_1$ and $y_2 = -y_1$. The depths to the top and bottom are z_1 and z_2, respectively. To keep the temperature of the earth's surface constant, the effect of a negative image source shown by dashed lines on Fig. 5 is added. In addition to these dimensions, the symbols appearing in the equations are:

t = time in seconds since emplacement of the body.

K = thermal conductivity in cal $cm^{-1}\,°C^{-1}\,sec^{-1}$.

k = thermal diffusivity = $K/c\rho$ where c is the heat capacity and ρ the density. We assume $c\rho = 0.55$.

T_z = the contribution of the intrusion to the bottom hole temperature in °C. It is 26.4°C at the depth of the wells (312 m) at location 148.

$Q_z = 5.56 \cdot 10^{-6}$ cal $cm^{-2}\,sec^{-1}$ is the heat flow along the vertical due to the intrusion as explained below.

S = 1374°C is the source strength.

The value of S is the difference between the original temperature of the

intrusion and the surface temperature, 26°C with an allowance for the heat of fusion. The temperature at the time of intrusion we assumed to be 1200°C. To take care of the heat of fusion we added 200°C for a total of 1400°C from the following argument. Heat of fusion = 90 cal/g × 2.6 = 234 cal cm^{-3} (J.W. Hawkins, personal communication, 1979). If we use the figure for granite, $c\rho$ = 0.55, the temperature increase to take care of the heat of fusion is 234/0.55 = 425°C. We assumed that the diapir consists of 50% molten material, thus adding 200°C to the initial temperature of 1200°C.

The equations of Simmons (1967) are:

$$T_z = \frac{S}{8} E(x, x_1, x_2)\, E(y, y_1, y_2)[E(z, z_1, z_2) + E(z, -z_1, -z_2)] \tag{2}$$

$$Q_z = \frac{-KS}{4\sqrt{\pi kt}} E(x, x_1, x_2)\, E(y, y_1, y_2)(e^{-z_1^2/4kt} - e^{-z_2^2/4kt}) \tag{3}$$

and:

$$E(x, x_1, x_2) \equiv \operatorname{erf}\frac{x - x_1}{\sqrt{4kt}} - \operatorname{erf}\frac{x - x_2}{\sqrt{4kt}} \tag{4}$$

to which we add the condition:

$$E_x \equiv E(x = 0, x_1, x_2) = 2E(x = 2.5 \text{ km}, x_1, x_2) \tag{5}$$

Starting with eq. 2, T_z is the contribution of the intrusion to the average measured temperature at the average depth of the eight wells at location 148, z = 312 m. The average gradient in the five wells surrounding location 148, viz locations 147, 146, 144, 151, and 152 is 3.82 ± 0.53°F/100 ft (Fig. 3, Table IV). Subtracting this from the gradient at location 148 which is 8.47°F/100 ft (Table IV) and multiplying by the depth of 1024 ft (312 m) gives T_z = 26.4°C. In eq. 3, Q_z is the contribution of the intrusion to the heat flow at location 148. Averaging the heat flow at the same surrounding locations gives 3.26 HFU which when subtracted from 8.82 HFU at location 148, leaves Q_z = 5.56 HFU.

Since we do not know the exact way the heat flow decreases away from the origin, we have assumed by eq. 5 that it drops to half value at x = 2.5 km. Equation 5 holds for a limited range of x_2 and kt. For the practical ranges of these quantities we have arbitrarily chosen two points where the curve has some slope, x_2 = 2.3 km, and is not too steep, x_2 = 1.1 km. The corresponding values for kt are $1.0 \cdot 10^{10}$ and $2.05 \cdot 10^{10}$. Since the origin is over the center of the intrusion, $x_2 = -x_1$, making $E_{x=0} = 2 \operatorname{erf}(x_2/\sqrt{4kt})$ at x = 0 (Fig. 6). In the case of a square cross-section when $x_2 = y_2$, $E_x = E_y$. When, however, $x_2 \neq y_2$, E_y has to be calculated from eq. 4 by replacing x's with y's but using the value of kt appropriate to the chosen value of x_2.

The conductivity is not assumed, but is determined by the heat flow value Q_z and the temperature at the bottom of the wells T_z. It is obtained by

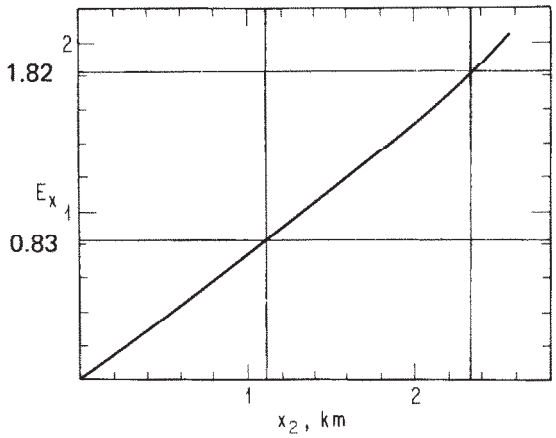

Fig. 6. $E_{x=0} = 2\ \mathrm{erf}(x_2/\sqrt{4kt})$ plotted against x_2, the half width in km for a chosen value of kt, obtained from Fig. 7.

dividing eq. 2 by eq. 3 and setting $z_2 = \infty$.

$$K = \frac{Q_z\sqrt{\pi kt}}{2T_z}\, E(z, z_1, -z_1) \exp\frac{z_1^2}{4kt} = 6.58 \cdot 10^{-3} \qquad (6)$$

So long as the values of the parameters are such that eqs. 2 and 3 are valid, the reader can verify by substituting numerical values, that K is independent of both kt and z_1. The range for kt for which this is true was determined from Fig. 7: $1.0 \cdot 10^{10} < kt < 2.05 \cdot 10^{10}$ and for z_1 from eq. 3: $0.5 < z_1 < 2.9$ km when $z_2 = \infty$. The calculated value of K is the only one that will satisfy both eq. 2 and eq. 3.

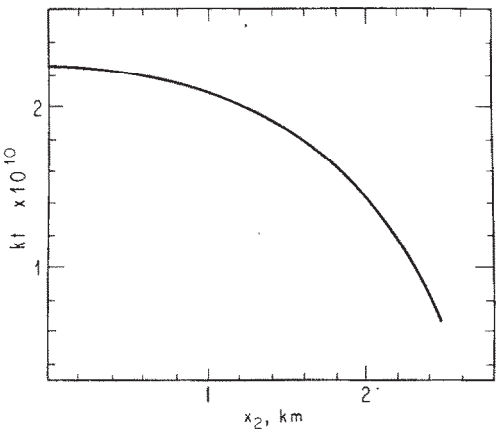

Fig. 7. The product kt — thermal diffusivity times the time elapsed since intrusion, plotted against the half-width x_2 in km for the condition that the amplitude of the anomalous heat flow at $x = 2.5$ km be half of its maximum value, as expressed by eq. 5.

Table VI lists the dimensions and the depth of burial for minimum and maximum ages of a few representative rectangular models pictured in Fig. 5. In Table VI, the values of z_2 were calculated from eq. 3 for arbitrarily chosen values of z_1:

$$z_2 = \left\{-4kt \ \ln\left[\exp\left(\frac{-z_1^2}{4kt}\right) - \frac{4Q_z\sqrt{\pi}}{KS} \ \frac{\sqrt{kt}}{E_x E_y}\right]\right\}^{1/2} \tag{7}$$

The maximum value of z_1 for a given kt pertains to a body of infinite depth extent, i.e. when the square bracket in eq. 7 is zero, $z_2 = \infty$.

DISCUSSION

We interpret the small value of conductivity of 6.58 mcal cm^{-1} °C sec when compared to the measured value of 12.55 for basement rocks in Table II to the negative temperature coefficient of quartzitic formations. Basalt and gabbro have a conductivity of 4.5 which is nearly constant between 0 and 400°C, which rules them out except as sporadic occurrences (Birch and Clark, 1940, fig. 5). According to Kanamori et al. (1968), the conductivity of quartz has a broad minimum and is fairly constant at 7.3 mcal cm^{-1} °C sec between 350 and 950°C. Beyond this temperature, radiative heat transport takes over and the conductivity rises again.

By projecting the gradient calculated from the total measured heat flow, we obtain the present average temperature at the depth of the models of Table VI. If we include the temperature at the surface, the bottom of the wells is at 74°C. The temperature gradient below 312 m, Q/K = 134°C/km. Take for example the bottom of model no. 3 of Table VI which is at 3.13 km. The average temperature for the region between this depth and the depth of the wells is $\frac{1}{2}[(74 \times 2) + (3.13 - 0.312)\ 134] = 263$°C. By scaling the curves for quartz in Fig. 2 of Birch and Clark (1940), we find that its conductivity at 263°C is about 0.57 of what it is at 25°. By multiplying our measured value of 12.55 in Table II by this factor, we get 7.2 mcal cm^{-1} °C sec for K, which is close enough to the calculated value of 6.58, especially if we take into account that the average temperature in the past was higher than at present. Thus, it is likely that quartz is a major constituent of the basement rocks below sampling depth.

As previously mentioned, the dependence of the temperature gradient and of the heat flow on the depth to the basement, so well brought out in Fig. 4 and Table V, is too large to be interpreted as resulting from a recent cooling of the climate. It must be caused in large part by the great conductivity contrast between the sediments and the pre-Tertiary basement rocks along with the steepness of the block-faulted structures of the basin. On Fig. 4, the point corresponding to the field at location 148 is way off the average slope to the right, suggesting the presence of an additional source of heat that we tried to model.

The Geothermal Gradient Map of the southeast Asia (SEAPEX, 1977)

TABLE VII

Average heat flow in five sedimentary basins of Sumatra and Java from temperature gradients of the SEAPEX map multiplied by $5 \cdot 10^{-3}$ cgs, the average thermal conductivity found in the central basin of Sumatra

Basin	Temperature gradient — avg. value (°F/100 ft) *	Number of wells	Heat flow (HFU)
North Sumatra	2.77 ± 0.53	23	2.52
Central Sumatra	3.26 ± 0.67	23	2.97
South Sumatra	2.75 ± 0.58	34	2.51
Sunda	2.80 ± 0.93	13	2.55
West Java	2.68 ± 0.56	19	2.44
East Java	2.26 ± 0.38	25	1.88

* Multiply by 18.23 for °C/km.

gives a general picture of the heat flow in the sedimentary basins of Java and Sumatra shown on Fig. 1. The average geothermal gradient in the Central Sumatra basin calculated from the 23 wells appearing on this map is 3.26° F/100 ft (59.8°C/km). This value is close to the value of 3.56 + 0.53° F/100 ft we got from 144 wells in the same areas. There is no reason to expect that the average thermal conductivity in the other basins of Java and Sumatra is substantially different from the one we found in the Central Sumatra basin. The poorly conducting shales which make up a substantial part of the geologic section determine to a large extent the average thermal conductivity. We can expect the average conductivity to lie well within 4 and $6 \cdot 10^{-3}$ cgs. As previously noted, the average thermal conductivity of $4.83 \pm 0.31 \cdot 10^{-3}$ cgs that we measured in Central Sumatra is probably smaller than the actual one because it excludes heat transfer by circulation of ground water in the upper portion of the section. Table VII gives the average heat flow in the sedimentary basins of Sumatra and Java from averages of the temperature gradients listed on the SEAPEX map on the assumption that the thermal conductivity is $5 \cdot 10^{-3}$ cgs. Heat flow appears to be uniform between 3.0 and 2.5 HFU from the North Sumatra basin to 110° E longitude. East from there it decreases, but the data points beyond 114° E become too sparse to average. Until the thermal conductivities are measured in the other basins, the differences in the heat flow in Table VII cannot be regarded as significant.

Where measurements of geothermal gradient have been made, the heat flow back of the Sunda Trench is high, which shows that there need not be secondary spreading in a deep marginal sea for the heat flow to be high. The absence of marginal seas north of the Sunda island arc rests on recent geologic observations. Hamilton (1979) has constructed a new tectonic map on which a feature of the granitic basement can be traced from Java to Kaliman-

tan across the Java Sea, so that if one stripped off the sediments to the northwest of this feature which would encompass most of the Java Sea, one would expose the Cretaceous granite of an old continental margin.

In other parts of the world where the landward plate is moving toward the trench, the subduction of "Andean" type of Uyeda and Kanamori (1979), the heat flow is not always high. Back of the Andes in Lake Titicaca it is 1.1 HFU (Sclater et al., 1970) and the average temperature gradient in 73 oil fields in Bolivia is only 0.8°F/100 ft (14.6°C/km) (Cueto and Aliaga, personal communication, 1971). Watanabe et al. (1977) show the heat flow in the Aleutian basin close to the world average.

Since there is no accepted explanation for epeirogeny, if one feels the need to ascribe the appearance of high heat flow back of an island arc to crustal tension, one might link periodic transgressions and regressions of epicontinental seas recorded in the sediments of the basin to periodic tension and compression. If the sum of the tension episodes is smaller than the sum of compressions, no marginal sea will be formed back of the arc. A highly speculative hypothetical mechanism for increasing the heat flow back of subduction appears in Fig. 8. It proposes that lava mobilized by entrainment of water generates diapirs which cause andesitic volcanism at the edge of the basin nearest to the subducting slab. Farther to the NE, the lava solidifies

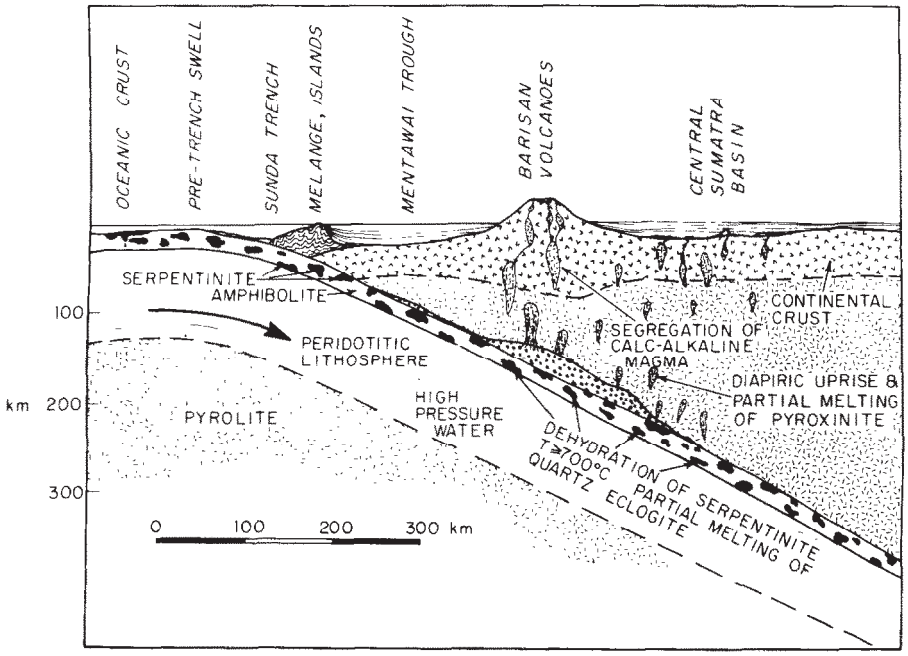

Fig. 8. Subduction at the Sunda island arc opposite Sumatra after Katili (1975) and Ringwood (1977). Magmatic diapirs have risen under the Central Sumatra basin.

before reaching the surface, thus delivering heat at shallow depths. Faulting of the landward plate in the geologic past and recent tectonic activity along the Semangka Fault may have facilitated the penetration of the basement by the diapirs.

ACKNOWLEDGEMENTS

We thank Ir. N. Kusnandar, who, although not an author of this paper, has contributed as much to this work as we did. We also thank the management of P.T. Caltex Pacific Indonesia at Rumbai, Penkanbaru, who generously provided all the data used in this study as well as manpower, laboratory facilities and subsistence during our stay in Rumbai. We thank the Management of Pertamina for permission to publish this paper and, in particular, Dr. Ismet Akil, Permanent CCOP Representative for Indonesia, who organized the project. The Introduction and Discussion sections of this paper benefited from conversations with R.N. Anderson and T.H. Jordan. Kenneth C. Macdonald and D.L. Williams reviewed an early version of the manuscript. We are particularly grateful to Seiya Uyeda for a thorough final review and for his suggestions regarding the bearing of our data on island arc tectonics. The construction of the thermal conductivity instrument donated to Pertamina and partial support for Carvalho and Vacquier was financed by IDOE under NSF Grant OCE 76-05542 to the University of California, San Diego. Carvalho was supported in large part by Conselho Nacional de Desenvolvimento Científico y Technológico CNPq, Brazil. This paper is a contribution of the Scripps Institution of Oceanography, new series.

Appendix: THERMAL CONDUCTIVITY INSTRUMENT

The instrument used for measuring the thermal conductivity is an adaptation of the one described by Von Herzen and Maxwell (1959) still used for measurements on ocean bottom sediments. The sensor is sold commercially by Fenwall Electronics, Framingham, Mass. (catalog number K1137A). It consists of a hypodermic needle 1 mm in diameter and 6.3 cm long containing throughout its whole length a loop of heater wire with a resistance of 356 Ohms. A thermistor having a resistance of about 1000 Ohms at 25°C is also located inside the needle 2.5 cm from its tip. The four wires are brought out to a 5-pin plug held by a cylindrical steel housing welded to the needle. The heater wire and the thermistor are fastened to the inner wall of the needle with Epoxy cement. The needle is mounted so it is flush with the surface of the broad face of a rectangular block of heat insulating material 9 × 9 × 3 cm, which consists of microspheres of glass filled with air and cemented together with Epoxy. This material is used for floating oceanographic instruments from the greatest ocean depths. Its density is 0.52 g cm^{-3}, its thermal conductivity is $0.22 \cdot 10^{-3}$ cal cm^{-1} $°C^{-1}$ sec^{-1} and its heat capacity 0.039 cal g^{-1} $°C^{-1}$ making the thermal diffusivity 0.00109, which is much smaller than the diffusivity of the average rock of about 0.011.

In the theory of heat conduction, the needle is represented by an infinitely long heat source emitting q calories per cm length per sec. The rate of rise of temperature of such a source when it is surrounded by an infinite medium is linearly proportional to the natural logarithm of time (Carslaw and Jaeger, 1959, p. 345; Blackwell, 1954). The thermal con-

ductivity of an infinite medium:

$$K = \frac{q}{4\pi} \frac{\ln(t_2/t_1)}{T_2 - T_1} \qquad \text{(A-1)}$$

where q is in cal per sec per cm length of the linear source, T_2 and T_1 are temperatures at times t_2 and t_1 after the heater current had been turned on. In the case of the half space, this formula gives only one half of the true value of K if we neglect the heat that diffuses into the microsphere plastic. In our latest experiments with this method the mean factor by which the experimental values need to be multiplied is within 5% of 2. Actually other sources of error more difficult to evaluate than the heat diffusing into the plastic enter into play, like the leakage of heat into the body housing the connector and the flow of heat toward the thermistor from portions of the needle not covered by the specimen which become much hotter than the part of the needle that is so covered. This important source of error is much reduced if the measurement is made in a shallow tray containing light lubricating oil which covers the surface of the probe and which also serves to make a good and uniform contact with the specimen. Practice has shown that the specimen need not have a special shape or cover the whole length of the needle. The flat surface of the sample should extend at least 1 cm all around the position of the thermistor and the sample should be at least 1 cm thick. The actual value of the number that is used to multiply the conductivity obtained from the formula for the infinite medium is obtained statistically for each needle from measurements on specimens previously measured in a divided bar apparatus.

The electrical measurements involved are extremely simple. The control box contains a regulated d.c. power supply for feeding both the heater and the thermistor circuits. The heater current can be adjusted between 25 and 50 mA. It is measured by a good quality needle meter. For the measurement of temperature, the voltage drop across the thermistor is compared to the voltage drop across an adjustable resistor by a high-resistance recording millivoltmeter on a paper chart 10 inches wide. As the needle heats up, the resistance of the thermistor decreases nonlinearly. To circumvent this inconvenience, a ballast resistor of about 450 Ohms is connected in series with the thermistor, so that when the resistance of the thermistor decreases, the current rises to make up for the nonlinearity. Over the range of temperatures used in the measurements, the voltage drop across the thermistor is inversely proportional to the temperature, the constant being about 8 mV per °C for the safe value of the current of about 0.5 mA. This constant was determined in a thermostated bath for each sensor. From eq. A-1 it is evident that on semilog paper a plot of millivolts on the linear scale against time on the logarithmic scale will yield a straight line the slope of which when multiplied by the heat supplied per cm and all the instrumental constants, gives the thermal conductivity. In practice it was found that it is sufficient to read the record at just two fixed times. All the constants are then lumped together and the result divided by the difference of the two voltage readings. The curves were read at 0.7 and 1.5 min after the heater current is switched on. Using three sensors, two men can process about 15 samples per hour.

A smooth saw cut is sufficiently flat for the measurement. In the case of loosely consolidated specimens we used a rotating lap with carborundum grit in oil. The specimens were immersed in a bucket containing a mixture of oil and kerosene, the liquid used for cooling the saw, and left to stand overnight in the air conditioned laboratory where the measurements were made. This procedure and the use of several sensors help to reduce temperature drifts.

REFERENCES

Anderson, R.N., Uyeda, S. and Miyashiro, A., 1976. Geophysical and geochemical constraints at convergent plate boundaries. I. Dehydration of the downgoing slab. Geophys. J. R. Astron. Soc., 44: 333—357.

Beck, A.E., 1976. The use of thermal resistivity logs in stratigraphic correlation. Geophysics, 41: 300—309.
Birch, F. and Clark, H., 1940. The thermal conductivity of rocks and its dependence upon temperature and composition. Am. J. Sci., 238: 529—635.
Blackwell, J.H., 1954. A transient flow method for determination of thermal constants of insulating materials in bulk. J. Appl. Phys., 25: 137—144.
Carlslaw, H.S. and Jaeger, J.C., 1959. Conduction of Heat in Solids. University Press, Oxford, 510 pp.
Carvalho, H. da S. and Vacquier, V., 1977. Method for determining terrestrial heat flow in oil fields. Geophysics, 42: 584—593.
Conaway, J.G. and Beck, A.E., 1977. Fine scale correlation between temperature gradient logs and lithology: Geophysics, 42: 1401—1410.
Dowdle, W.L. and Cobb, W.M., 1974. Estimation of static formation temperature from well logs. 49th Annu. Meet. Soc. Pet. Eng. of AIME, Fall Meet., Houston, 8 pp.
Fitch, T., 1970. Earthquake mechanisms and island arc tectonics in the Indonesian Philippine region. Bull. Seismol. Soc. Am., 60: 565—591.
Hamilton, W., 1977. Subduction in the Indonesian region. In: M. Talwani and W. Pitman III (Editors), Island Arcs, Deep Sea Trenches and Back-Arc Basins. Maurice Ewing Ser., 1, Am. Geophys. Union, Washington, D.C., pp. 15—31.
Hamilton, W., 1979. Geology of the Indonesian Region. U.S. Geol. Surv., Profess. Pap., 1078: 345 pp.
Kanamori, H., Fujii, N. and Mizutani, H., 1968. Thermal diffusivity measurements of rock-forming minerals from 300° to 1100°K. J. Geophys. Res., 73: 595—605.
Katili, J.A., 1975. Volcanism and plate tectonics in the Indonesian island arcs. Tectonophysics, 26: 165—188.
Lister, C.R.B., 1972. On the thermal balance of a mid-ocean ridge. Geophys. J. R. Astron. Soc., 26: 515—535.
Mertosono, S., 1975. Geology of Pungut and Tandun Oil Fields, Central Sumatra, P.T. Calex Pacific Indonesia, Rumbai, Pekanbaru.
Mertosono, S. and Nayoan, G.A.S., 1974. The Tertiary Basinal Area of Central Sumatra. 3rd Conv. Indones. Pet. Assoc., Jakarta.
Morgan, W.J., 1971. Plate Motions and Deep Mantle Convection. Geol. Soc. Am. Mem., 132 (Hess Vol.).
Ringwood, A.E., 1977. Petrogenesis in island arc systems. In: M. Talwani and W. Pitman III (Editors), Island Arcs, Deep Sea Trenches and Back-Arc Basins. Maurice Ewing Ser., 1, Am. Geophys. Union, Washington, D.C., pp. 311—324.
Sclater, J.G., Vacquier, V. and Rohrhirsch, J.H., 1970. Terrestrial heat flow measurements on Lake Titicaca. Earth Planet. Sci. Lett., 8: 45—54.
SEAPEX, 1977. Geothermal Gradient Map of Southeast Asia. SE Asia Petroleum Exploration Society, Cities Service Oil Co., Singapore.
Simmons, G., 1967. Interpretation of heat flow anomalies. 2. Flux due to initial temperature of intrusives. Rev. Geophys., 5: 109—120.
Vacquier, V. and Taylor, P.T., 1966. Geothermal and magnetic survey off the coast of Sumatra. Bull. Earthquake Res. Inst., 44: 531 - 540.
Von Herzen, R.P. and Maxwell, A.E. 1959. The measurement of the thermal conductivity of deep sea sediments by the needle probe method. J. Geophys. Res., 64: 1557—1563.
Watanabe, T., Langseth, M.G. and Anderson, R.N., 1977. Heat flow in the back-arc basins of the Western Pacific. In: M. Talwani and W. Pitman III (Editors), Island Arcs, Deep Sea Trenches and Back-Arc Basins. Maurice Ewing Ser., 1, Am. Geophys. Union, Washington, D.C., pp. 137—161.
Weiss, R.F., Lonsdale, P.F., Lupton, J.E., Bainbridge, A.E. and Craig, H., 1977. Hydrothermal plumes in the Galapagos Rift. Nature, 267: 600—603.
Williams, D.L., Von Herzen, R.P., Sclater, J.G. and Anderson, R.L., 1974. The Galapagos spreading center, lithospheric cooling and hydrothermal circulation. Geophys. J. R. Astron. Soc., 38: 587.
Uyeda, S. and Kanamori, H., 1979. Back-arc opening and the mode of subduction. J. Geophys. Res., 84: 1049—1061.